Available online at www.sciencedirect.com

ScienceDirect

Procedia Structural Integrity 1 (2016) 010–017

Structural Integrity Procedia

www.elsevier.com/locate/procedia

XV Portuguese Conference on Fracture, PCF 2016, 10-12 February 2016, Paço de Arcos, Portugal

Fracture mechanics based determination of the fatigue strength of weldments

U. Zerbst [a]*, M. Madia [a] and B. Schork [b]

[a] *BAM-Federal Institute for Materials Research and Testing, 9.1, Unter den Eichen 87, D-12205 Berlin, Germany*
[b] *Technische Universität Darmstadt, MPA/IFW, Grafenstraße 2, D-64283 Darmstadt, Germany*

Abstract

A fracture mechanics model which shall be applied to the fatigue strength determination of weldments has to focus on various aspects such as: (a) the description of mechanical and physical short fatigue crack extension which is characterised by yielding conditions which do not permit the application of the common ΔK concept and by the gradual build-up of the crack closure effect, (b) a consistent methodology for determining the initial crack size, (c) based on this, the determination of a fatigue limit, (d) the treatment of multiple crack propagation at load levels above this limit, (e) the variation of the local geometry along the weld toe, and (f) statistical effects. The paper gives a limited overview of the work the authors did in this field during the last years within the German project cluster IBESS. A model is presented and briefly discussed which covers the questions above.

Peer-review under responsibility of the Scientific Committee of PCF 2016.

Keywords: Weldments, fatigue strength, fracture mechanics, fatigue crack propagation

1. Stages of the lifetime of a component subjected to cyclic loading

The fatigue lifetime of a component subjected to cyclic loading can be roughly subdivided into three stages: crack initiation, fatigue crack propagation and fracture. Frequently, the initiation stage is seen as the phase during which the crack is nucleated and subsequently extended to a size externally visible. However, on closer look, it may be further subdivided into the actual initiation phase characterized by the accumulation of plastic deformation frequently at defects such as inclusions, pores etc. and the subsequent phase of short crack propagation Murakami (2002). Note that the early crack propagation and arrest of microstructurally short cracks forms the background of the fatigue life phenomenon Miller (1999). At stress levels higher than the endurance limit a limited number of cracks will further propagate and develop to what is designated as mechanically/physically short cracks. In contract to the micromechanically short cracks the size of which is in the order of micromechanical features such as the grain size, mechanically short cracks are comparable in size to the plastic zone ahead of its tip.

* Corresponding author.
E-mail address: uwe.zerbst@bam.de

Peer review under responsibility of the Scientific Committee of PCF 2016.
10.1016/j.prostr.2016.02.003

They can be described by continuum mechanics-based fracture mechanics, however not by the linear-elastic ΔK concept because the plastic zone size is in the order of the crack size. Instead, the crack driving force has to be given as an elastic-plastic parameter. The specific meaning of the term "physically short" is that the crack closure mechanism is not yet fully developed but gradually increases from no closure effect of the initial crack to a constant value when the crack reaches the size of the so-called long crack. The propagation of the latter can be described by the common da/dN-ΔK curve concept. Usually the propagation phase of the mechanically and physically short crack, the sizes of which roughly overlap, constitutes the major part of fatigue life.

2. The Model

2.1 Elastic-plastic cyclic crack driving force

Following a proposal of McClung (1997) the cyclic J integral is determined by

$$\Delta J = \frac{\Delta K^2}{E'} \cdot \left[f\left(\Delta L_r\right) \right]^{-2} \tag{1}$$

with the ligament yielding correction term $f\left(\Delta L_r\right)$, deviating from the original, being defined by

$$\Delta L_r = \frac{\Delta \sigma_{app}}{2 \cdot \sigma_0} . \tag{2}$$

In Eqn. (2) the parameter $\Delta\sigma_{app}$ is the applied cyclic load and σ_0 is what the authors call a reference yield load which they use instead of the common limit load and for which they provide parameter equations in Madia (2014). For the further use in the fatigue crack propagation analysis, ΔJ is formally converted to ΔK_p with the index "p" standing for "plasticity corrected". With respect to the ligament yielding correction function $f(L_r)$ the method makes use of the common equations, e.g. in R6, Revision 4, (2009):

$$\Delta K_p = \sqrt{\Delta J \cdot E'},\ E' = \begin{cases} E & \text{plane stress} \\ E/\left(1-\nu^2\right) & \text{plane strain} \end{cases} \tag{3}$$

2.2 Gradual build-up of the crack closure effects

Crack closure means that the crack, during unloading, closes above zero stress level. The effect is caused by a number of mechanisms with the plasticity-induced, the roughness-induced and the oxide-induced are the most important ones Suresh (1998), for a more detailed discussion see Zerbst (2006). It is commonly expressed by a closure term U:

$$U = \Delta K_{eff} / \Delta K \tag{4}$$

Figure 1 illustrates the gradual build-up of the crack closure effect with increasing crack size. Up to the initial crack depth a_i, which approximately marks the transition from the microstructurally to the physically short crack (in reality there is a range), U=1, i.e., no closure effect exists. Then, U gradually decreases with increasing crack length until it reaches the constant value U_{LC} of the long crack phase. The determination of U(a) by the present model makes use of the fact that this is mirrored in the development of the fatigue crack initiation threshold ΔK_{th} such as illustrated in Figure 2 and described by an equation

$$\frac{U(a)-1}{U_{LC}-1} = \frac{\Delta K_{th}(a) - \Delta K_{th,eff}}{\Delta K_{th,LC} - \Delta K_{th,eff}} \tag{5}$$

The crack depth dependency of the threshold ΔK_{th} is designated as cyclic R curve. It is illustrated in more detail in Figure 3. Note that ΔK_{th} can be interpreted as consisting of two components, the intrinsic $\Delta K_{th,eff}$ which is a material parameter dependent on the stiffness properties (mainly the E modulus) of the material (cf. Zerbst (2006)) and a crack depth dependent component $\Delta K_{th,op}$ which reflects the crack closure effect.

$$\Delta K_{th} = \Delta K_{th,eff} + \Delta K_{th,op} \tag{6}$$

It is $\Delta K_{th,op}$ which reaches an upper bound when the physically short crack transforms into the long crack. Note that $\Delta K_{th,eff}$ is identical to the closure-free ΔK_{th} at high R ratio. Note further that the U function, in a component, does not start at a = 0 but at a = a_i and that the cyclic R curve does not begin at ΔK_{th} = 0 but at $\Delta K_{th} = \Delta K_{th,eff}$.

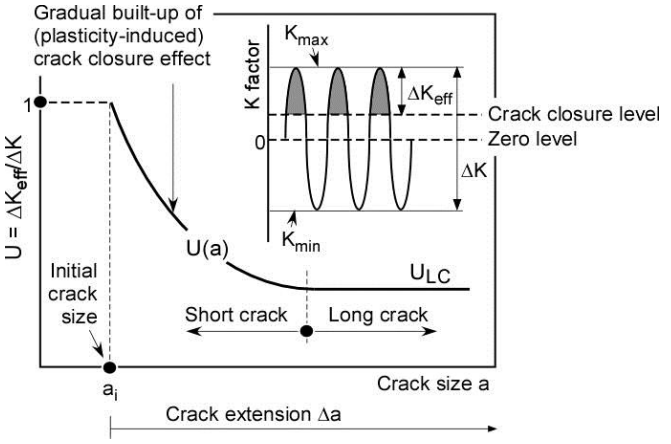

Fig. 1: Gradual build-up of the crack closure effect, schematic view.

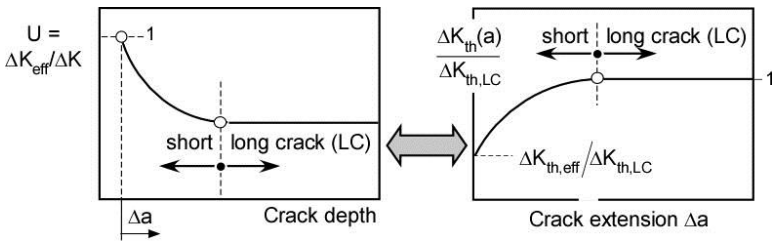

Fig. 2: Parallel development of the closure parameter U and the fatigue crack propagation threshold with increasing crack depth, schematic view.

As can be seen from Eqn. (5), the determination of U(a) in the physically short crack range among other data requires the information on the crack size independent long crack value U_{LC}. The latter is given by

$$U_{LC} = \left(1 - \sigma_{op}/\sigma_{max}\right)/\left(1 - R\right) \tag{7}$$

with the function σ_{op}/σ_{max} being obtained by Newman's (1984) approach which is also realized in the widely used NASGRO (2000) software. Deviating from the original approach, σ_{max}/σ_f within the set of parameter equations is replaced by

$$\frac{K_{max}}{K_{Y,cyc}} = \frac{Y \cdot \sigma_{max} \cdot \sqrt{\pi \cdot a}}{\sigma_{Y,cyc} \cdot \sqrt{\pi \cdot a}} = \frac{Y \cdot \sigma_{max}}{\sigma_{Y,cyc}} \tag{8}$$

this way allowing for a wider application field with respect to the loading type (tension, bending), McClung (1994)

and instead of the static flow stress $\sigma_f = 0.5\ (\sigma_Y+R_m)$ the cyclic yield strength $\sigma_{Y,cyc}$ is applied. The parameters C, m, p and $\Delta K_{th,LC}$ are empirical coefficients and parameters which have to be experimentally determined. The long crack threshold $\Delta K_{th,LC}$ as well as the cyclic R curve are dependent on the load ratio R.

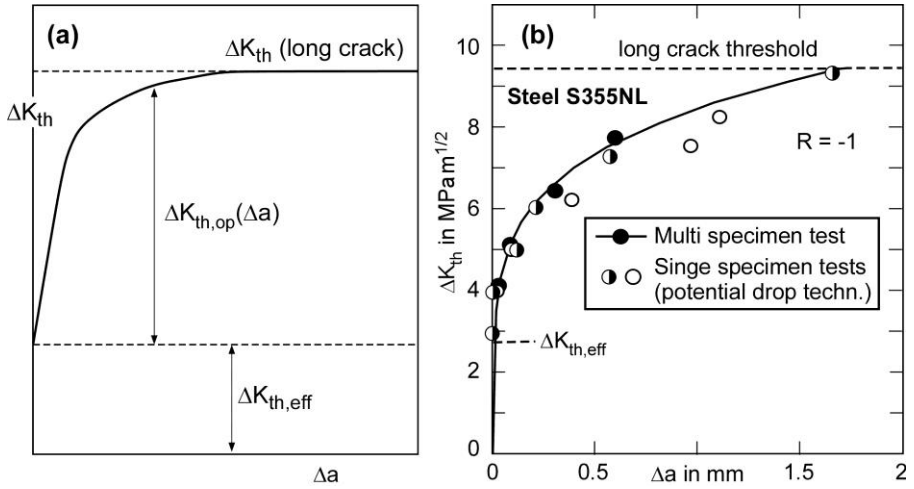

Fig. 3: Cyclic R curve. (a) Schematic view; (b) Example Zerbst (2015)

Finally the crack propagation rate da/dN is determined by

$$\frac{da}{dN} = \begin{cases} C\cdot\left[U(a)\cdot\Delta K_p\right]^m\cdot\left[1-\dfrac{\Delta K_{th,LC}}{\Delta K_p}\right]^p & \text{short crack} \\ C\cdot\left[U_{LC}\cdot\Delta K_p\right]^m\cdot\left[1-\dfrac{\Delta K_{th}(a)}{\Delta K_p}\right]^p & \text{long crack} \end{cases} \tag{9}$$

2.3 Determination of the initial crack

With respect to the initial crack size a_i a case distinction is necessary: (a) Sometimes large defects (large non-metallic inclusions, slag inclusions in weldments etc.) are existent which, because of poor cohesion in the matrix material, can immediately be treated as initial cracks. An example of an aluminium alloy is provided by the authors in Zerbst (2011).However, many other materials including high quality weldments do not show such large defects. There will also be crack initiation, e.g., at non-metallic inclusions but the microstructurally short cracks will arrest at grain boundaries or other microstructural features after some growth. The fatigue limit defines the transition from the arrest of all cracks to the propagation of just one crack to the size of a mechanically/physically short crack. Within the present model the size of the crack which just no longer is arrested at fatigue strength level is determined as a_i Zerbst (2015). The principle is illustrated in Figure 4(a). The analysis is based on a cyclic R curve approach. This is similar to the R curve concept in static fracture mechanics with the difference that the tangency criterion does not provide the information on the transition from stable to unstable crack extension but from arrest to non-arrest of the cyclic growing crack. The crack driving force in terms of ΔK_p is simulated for a tension loaded smooth specimen containing just one semicircular crack as it refers to the situation at the fatigue limit. With further increasing stress level the number of non-arrested cracks is increasing. That this idea is reasonable, demonstrates Figure 4(b,c). First it can be seen that the number of cracks really corresponds to the load level. When the curves, both for all cracks and for cracks with a depth larger than 50 µm, are extrapolated to a stress amplitude of about 100 MPa, which approximately refers to the fatigue limit of the tested weldment, it really points to the order of just zero to one crack.

Let's come back to Figure 4(a): The crack driving force in the smooth specimen, ΔK_p, is determined for the load level that refers to the material fatigue limit which, if not otherwise available, can been estimated from the ultimate tensile strength. The applied ΔK_p is obtained as a function of the crack depth a. In the next step, the cyclic R curve is introduced. Its minimum value at the ordinate is given by the intrinsic threshold $\Delta K_{th,eff}$ because of which the only degree of freedom is its position at the abscissa. This is chosen such that the tangency criterion between the applied and the R curve is satisfied. After the latter is fixed this way, a_i is identified as its zero point at $\Delta K = \Delta K_{th,eff}$. For S355NL steel it was found to be $a_i \approx 17$ µm (mean value). Note again that the crack arrest based a_i is a lower bound and relevant for the fatigue life only as long as no larger initial defect exist.

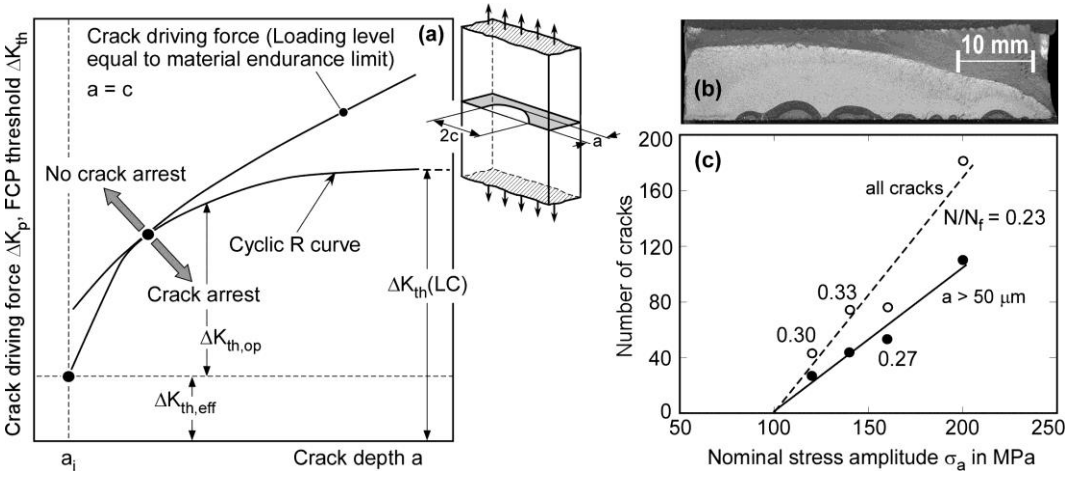

Fig. 4: (a) Cyclic R curve analysis for determining the initial crack size a_i of the material; (b) Example of marking the cracks by tempering; (b) Number of cracks as a function of the load level; (c) Number of cracks along the weld toe of the butt welds at 1/4 to 1/3 of the overall lifetime.

2.4 Fatigue limit and finite life fatigue strength

At stress levels above the fatigue limit, multiple cracking has to be modeled. For this purpose the weld toe is subdivided into equidistant sections such as shown in Figure 5(a). Each section is characterized by different local geometry parameters as input information for parametric equations for the stress-depth profiles. Alternatively, finite element based stress profiles can be used. The geometric parameters comprise the weld toe radius ρ, the flank angle α, the excess weld material h and the depth of secondary notches k (Figure 5b).

The allocation of the local geometry parameters to the sections is done in a stochastic way with an additional criterion for smoothing the transition from section to section. Each section contains a semicircular crack of depth a_i. Crack extension is simulated individually for depth and length-at-surface growth. Due to the different weld toe geometry from section to section, some cracks will grow faster, others slower and still others not at all. When the surface points of two cracks come close together, coalescence is simulated. The calculation is interrupted, when the maximum K_p in the loading cycle approaches the toughness or when the crack depth has reached a certain limit, e.g. half the plate thickness. In terms of a Monte Carlo analysis the calculation is repeated several times, first at the same load level and subsequently on other load levels. The result is a scatter band of S-N data such as in the experiment which finally can be statistically processed. The determination of the fatigue limit of the component follows the same philosophy as the determination of the initial crack depth above. What is different now is, that a_i and the cyclic R curve are the input parameters whereas the crack driving force curve $\Delta K_p(a)$, now for the weldment, is determined for iteratively changing load levels. The latter are introduced as statistical quantities and locally allocated to the equidistant sections. Consequently the determination of the fatigue limit is also carried out as a Monte Carlo simulation. At each run, an applied crack driving force curve $\Delta K_p(a)$ is determined for each section. The nominal stress corresponding to the applied curve of the section with the lowest stresses which meets the tangency criterion with the fixed cyclic R curve defines the fatigue limit of the weldment.

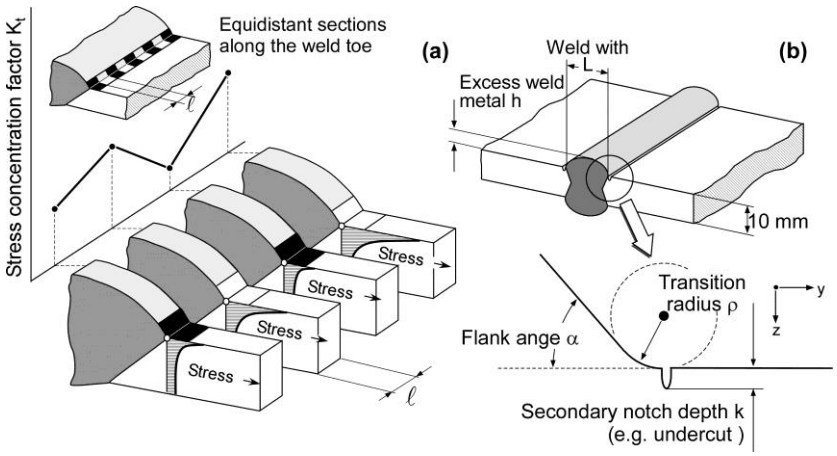

Fig. 5: (a) The division of the weld toe into equidistant sections. Each of it is characterized by its own weld geometry and stress-depth profile based on empirical statistical information. (b) The local geometry parameters at the weld toe considered by the model.

3. Parameter sensitivity analysis

Due to the limited space of this paper the following discussion will be limited to a few results only. Figure 6 shows experimental S-N points of a butt weld of steel S355NL (plate thickness: 10 mm; width: 50 mm) for a stress ratio of R = -1. The experimentally determined geometry parameters along the weld toe are provided in Table 1. The analysis was performed for varying section width ℓ according to Figure 5(a) which has to be treated as a model parameter due to a number of model simplifications (e.g., exactly one crack at the centre line of each section). As can be seen the results become more realistic when the section with ℓ becomes larger. However, further investigation is needed here, particularly since the slope of the predicted curve is smaller than the experimental one and also as those expected by the IIW reference curve, Hobbacher (2016) for the weld detail. The reason seems to be an overestimation of the ligament yielding effect by the model which is also indicated by ongoing comparison with finite element based ΔJ.

Table 1: Variation in the local weld toe parameters. Experimental data (line scans) statistically processed.

Parameter	50% probability	10% probability	90% probability	Distribution type
Transition radius ρ	0,87 mm	0,47 mm	1,61 mm	Lognormal
Flank angle α	31,9 °	24,4 °	39,4 °	Normal
Excess weld metal h	1,57 mm	1,33 mm	1,82 mm	Normal
Secondary notch depth k	62 μm	40 μm	83 μm	Normal

In addition, Figure 6 shows the statistical determination of the fatigue strength of the butt weld. This, in the present model, is defined as no fracture at and above 10^7 loading cycles. The stress level is pointwise increased and the number of fracture predictions at $N \leq 10^7$ is counted. The fracture probability is simply the ratio of fracture events and analysis runs.

Figures 7 and 8 illustrate the effect of the local geometry parameters of the weld toe on the S-N curve predicted by the present model. These are the weld transition radius ρ (Figure 7a), the excess weld metal h (Figure 7b), the flank angle α (Figure 8a) and the depth of secondary notches k (Figure 8b). It shows up that the effects in any case increase at lower load levels towards the fatigue limit. This is particularly true with respect to the secondary notch depth k. Whilst the effect of the excess weld metal h, in general, seems to be limited (although very small h-values have not been investigated) there is a clear trend with respect to the flank angle in that the fatigue strength becomes

progressively higher when α becomes smaller. Note however, that the various parameters will not be totally independent in real weldments. A problem on its own is the definition of the weld transition radius ρ which always will be a bit arbitrary. Like the other parameters it has been determined by line scans on the weldment surface. It was then defined as a rather global parameter, whilst the local variations in surface roughness are attributed to the secondary notches. It is too early for an in-depth discussion of all the parameters. Nevertheless, the examples demonstrate the usefulness of the model for predicting trends. As mentioned, only a small selection of the validation exercises within IBESS is presented here. The cluster project involved different weldment types (butt welds, cross joints and longitudinal stiffened plates), two steels (S355NL and S960QL) of quite different strengths, different weld geometries due to different welding techniques (WIG, MAG) and as-welded and stress relieved welds.

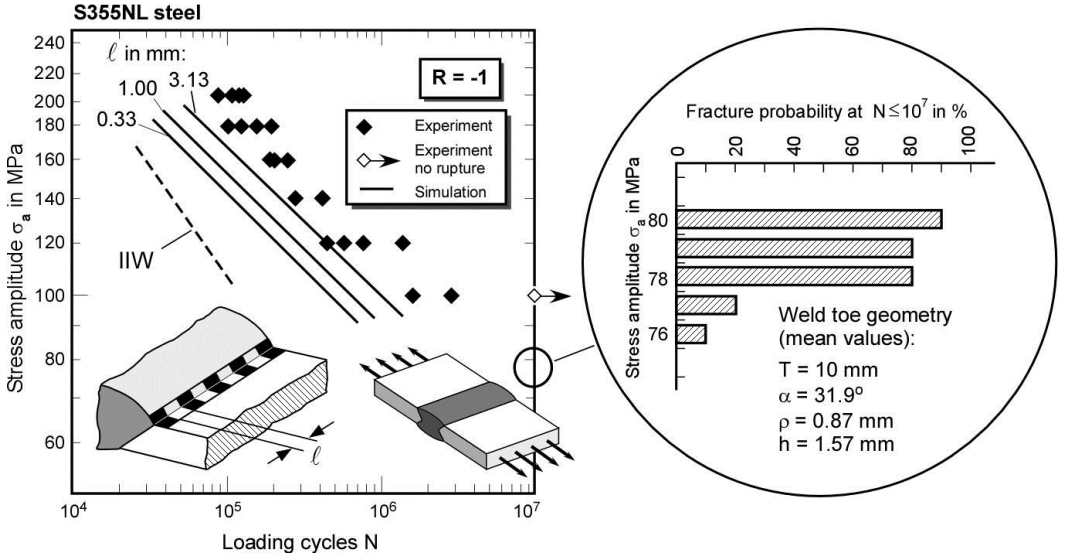

Fig. 6: Comparison of experimental S-N curve data of a butt welded plate with model predictions with different section widths ℓ as defined in Figure 5. Only the mean values of the analyses are shown.

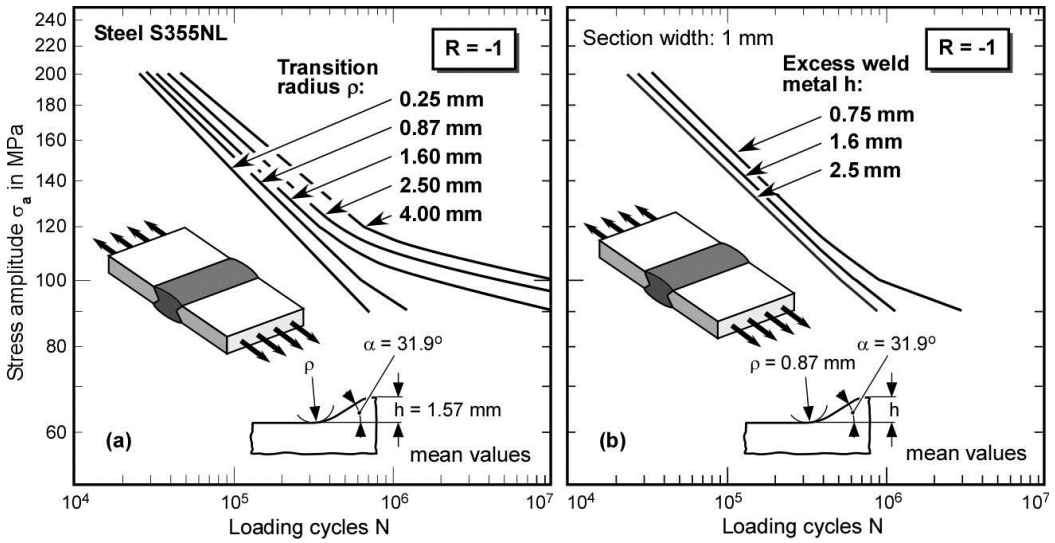

Fig. 7: Application of the present model to estimate the influence of weld toe geometry. (a) transition radius ρ; (b) excess weld metal h.

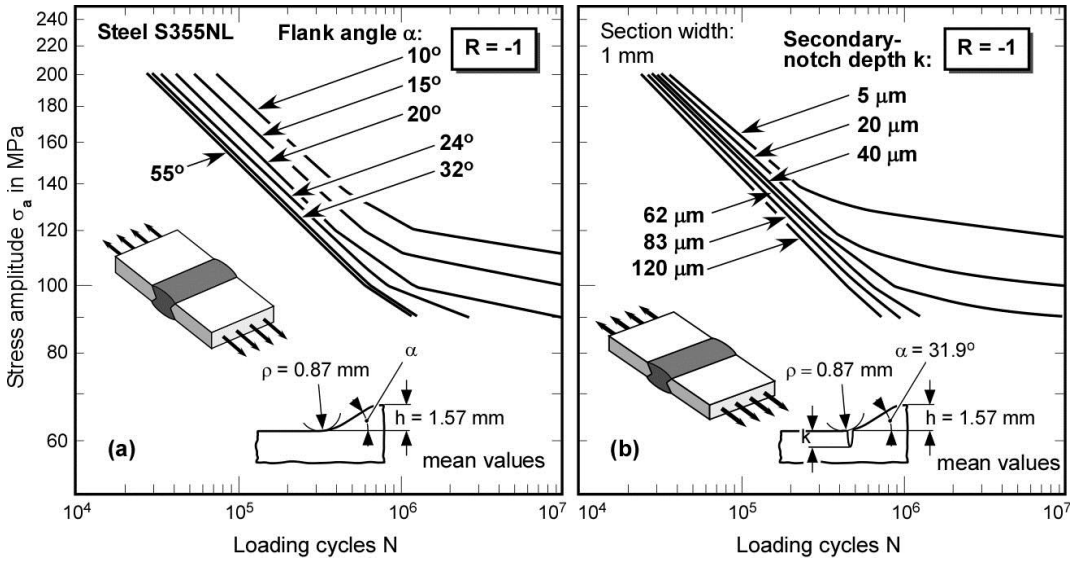

Fig. 8: Application of the present model to estimate the influence of weld toe geometry. (a) flank angle α; (b) secondary notch depth k.

4. Summary

An analytical fracture mechanics-based model for predicting the fatigue strength of weldments is presented. Characteristics are the elastic-plastic determination of the crack driving force, the determination of the gradual build-up of the crack closure effect, an option for determining the initial crack size based on a crack arrest criterion, the determination of the fatigue strength of components, the consideration of the varying weld geometry along the weld toe and the existence of multiple cracks at load levels above the fatigue limit. The application of the model is demonstrated at the background of a selected validation exercise. Finally the results of parameter analyses are presented.

References

Hobbacher, A., 2016. *Recommendations for fatigue design of welded joints and components* (formerly IIW Recommendations IIW 1823), Springer

Madia, M., Arafah, D., Zerbst, U., 2014. Reference load solutions for plates with semi-elliptical surface cracks subjected to biaxial tension loading. Int. J. Pres. Ves. Piping, 119, 19-28.

McClung, R.C, 1994. Finite element analysis of specimen geometry effects on fatigue crack closure. Fat. Fract. Engng. Mat. Struct. 17, 861-872.

McClung, R.C., Chell, G.G., Lee, Y.-D., Russel, D.A., Orient, G.E., 1997. A practical methodology for elastic-plastic fatigue crack growth. ASTM STP 1296, 317-337.

Miller, K.J., O'Donnel, W.J., 1999. The fatigue limit and its elimination. Fatigue Fracture Engng. Mater. Struct. 22, 545-557.

Murakami, Murakami, Y., 2002. *Metal Fatigue. Effects of Small Defects and Nonmetallic Inclusions*. Elsevier.

NASGRO, Fatigue crack growth computer program "*NASGRO*" Version 3, NASA, Houston, Texas, 2000.

Newman, J.C. Jr., 1984. A crack opening stress equation for fatigue crack growth. Int. J. Fracture. 24, R131-R135.

R6, Revision 4, 2009. Assessment of the Integrity of Structures Containing Defects. British Energy Generation Ltd (BEGL), Barnwood, Gloucester.

Suresh, S., 1998. *Fatigue of Materials*. Cambridge University Press, Cambridge et al., Section 7: Retardation of constant amplitude fatigue crack growth, 222-271.

Zerbst, U., Madia, M., Hellmann, D., 2011. An analytical fracture mechanics model for estimation of S-N curves of metallic alloys containing large second particles. Engng. Fracture Mech. 82, 115-134.

Zerbst, U., Madia, M., 2015. Fracture mechanics based assessment of the fatigue strength: Approach for the determination of the initial crack size. Fatigue Fracture Engng. Mat. Struct., 38, 1066-1975.

Zerbst, U., Vormwald, M., Pippan, R., Gänser, H.-P., Sarrazin-Baudox, C., Madia, M., 2016. About the fatigue crack propagation threshold of metals as a design criterion – a review. Engng. Fracture Mech. doi: http://dx.doi.org/10.1016/j.engfracmech.2015.12.002.